JOURNAL OF SOLID STATE CHEMISTRY **136,** 125–133 (1998)
ARTICLE NO. SC977683

An Electron Diffraction Study of Sn/P and Interstitial Ni Ordering in $Ni_{1+m}Sn_{1-x}P_x$ B8-type Solid Solutions

S. Furuseth,* A-K. Larsson,† and R. L. Withers†,[1]

*Department of Chemistry, University of Oslo, N-0315 Oslo 3, Norway; and †Research School of Chemistry, Australian National University, Canberra, Australian Capital Territory 0200, Australia

Received June 30, 1997; in revised form November 3, 1997; accepted November 7, 1997

Electron diffraction is used to investigate Sn/P and interstitial Ni atom ordering in the apparent wide range, non-stoichiometric $Ni_{1+m}Sn_{1-x}P_x$ ternary B8-type solid solution. Two complex modulated structures are found to exist in a limited area of the solid solubility range, described by compositions around $Ni_{1.1}Sn_{0.7}P_{0.3}$. This region of the high temperature $Ni_{1+m}Sn_{1-x}P_x$, B8-type phase field had previously been found to separate out as an isolated B8 type phase region at low temperatures. A complex, long range ordered triclinic superstructure phase is found for specimens quenched from lower temperatures and a plausible structural model, based on ordering of NiP_3Sn_2 trigonal bipyramidal clusters, proposed. The underlying B8 subcell remains metrically hexagonal so that there are at least 12 distinct twin variants whose B8 sublattice reflections overlap exactly. The diffraction patterns characteristic of specimens quenched from higher temperatures are compatible with a multiply twinned microdomain model. © 1998 Academic Press

1. INTRODUCTION

A large number of transition metal compounds with the general formula $T_{1+m}B$ (T a transition metal and B a chalcogen, a pnictide, or a member of the carbon or boron groups) are known. Such compounds frequently adopt the NiAs–Ni_2In (or B8) type structure (space group $P6_3/mmc$, T in Wyckoff positions 2a (fully occupied) and 2d (partially occupied), B in position 2c) and can be described as a (compressed) hexagonal close-packed array of B-atoms with all the octahedral sites occupied by T and the trigonal bipyramidal sites partially occupied by T (see Fig. 1). Many such B8-type phases are reported to be capable of existing over wide ranges of m intermediate between 0 and 1 (1–4). In addition to this variability in T/B ratio, it is known that it is possible to substitute both on the T and the B sites of such phases (1, 3, 5).

As a result of this compositional flexibility, considerable scope exists for studying the effect on structure and properties of substitution (both on T and B sites), and changing the T/B ratio. As a part of such studies, Furuseth and Fjellvåg (6) previously described the existence of an apparent wide range non-stoichiometric, $Ni_{1+m}Sn_{1-x}P_x$ ternary B8-type solid solution. The extent of this B8 solid solution field was strongly temperature dependent, decreasing markedly at lower temperatures, with a maximum extent given by $0.00 \le m \le 0.65, 0.00 \le x \le 0.32$ at higher temperatures (6). At lower temperatures, two separate B8-type phase regions with substantial Sn(P) substitution were found to exist, one centered around $m = 0.50$ and the other around $m = 0.10$.

The large difference in size between tin atoms and (the much smaller) phosphorus atoms suggests that there should exist a strong driving force for Sn/P ordering in these $Ni_{1+m}Sn_{1-x}P_x$, B8-type phase fields. A single crystal structure refinement of a related ternary line phase Ni_2SnP (5), in which exact Sn/P ordering was found, also supports the notion that Sn/P ordering in these B8-type solid solutions is highly likely. In addition to Sn/P ordering, there is also the possibility of ordering of the T atoms in the partially filled trigonal bipyramidal sites. It is now well known (4, 7–9) that a wide variety of modulated structures (superstructures as well as incommensurately modulated structures) occur within binary $T_{1+m}B$, B8-type phase fields as a result of ordering of filled trigonal bipyramidal sites and associated structural relaxation. On the basis of interatomic separation considerations, Furuseth and Fjellvåg (6) suggested that any Sn/P ordering would be strongly correlated with interstitial Ni ordering and that NiP_3Sn_2 trigonal bipyramidal clusters should be particularly stable.

Single crystal X-ray and powder neutron diffraction investigation of this $Ni_{1+m}Sn_{1-x}P_x$, B8-type phase field, however, failed to detect any evidence for ordering and found only the B8-type average structure—implying a random distribution of Sn and P atoms on the B sites and Ni atoms in the partially filled trigonal bipyramidal sites. The only indications for possible ordering were a diffuse intensity background in some parts of the neutron powder pattern and a somewhat less than satisfactory fit to the structure

[1] To whom correspondence should be addressed.

0022-4596/98 $25.00

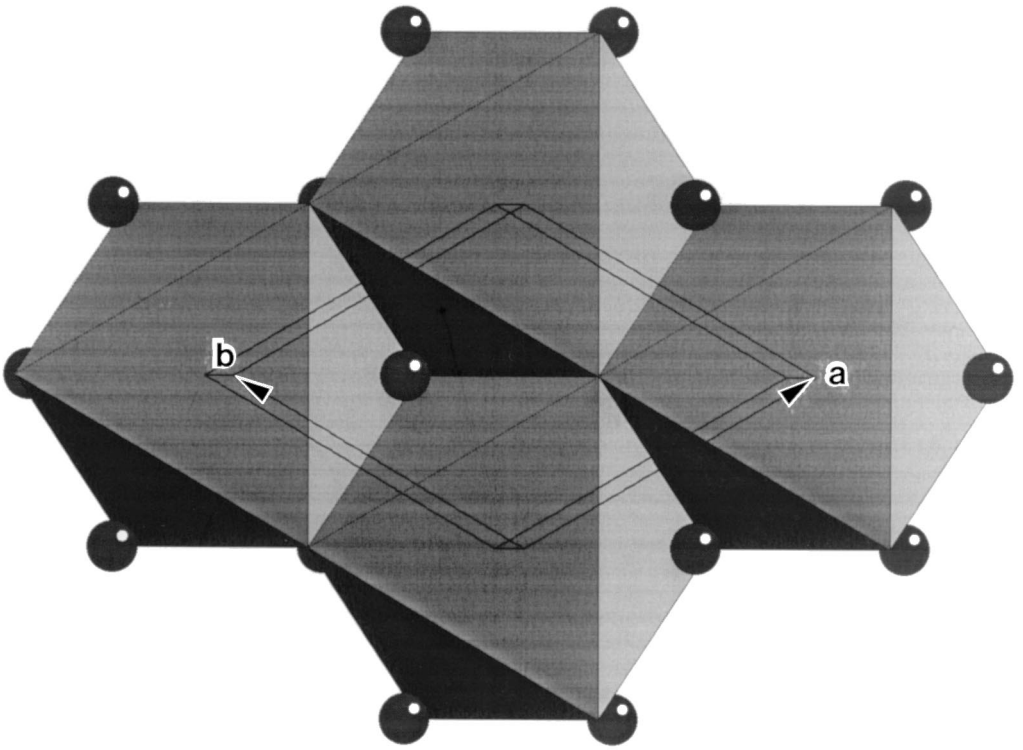

FIG. 1. Ideal B8-type $T_{1+m}B$ structure projected slightly away from [001]. Only atoms with z fractional coordinates between $\frac{1}{4}$ and $\frac{3}{4}$ are shown. The T_1B NiAs-type octahedral array is shown along with the partially occupied, interstitial T_m sites (shown as spheres). There are two c glide related such interstitial sites per B8 unit cell (E_a and E_b: E_a at $\mathbf{r}_a = \frac{2}{3}\mathbf{a} + \frac{1}{3}\mathbf{b} - \frac{1}{4}\mathbf{c}$ and E_b at $\mathbf{r}_b = \frac{1}{3}\mathbf{a} + \frac{2}{3}\mathbf{b} + \frac{1}{4}\mathbf{c}$). The B8 unit cell is outlined and the unit cell axes marked.

refinements (6). Given that the additional scattering arising from ordering and associated structural relaxation in such B8-type phase fields is often rather weak and difficult to detect with standard X-ray and neutron diffraction methods (4, 7–10), it was decided to undertake a systematic study of the ternary $Ni_{1+m}Sn_{1-x}P_x$ solid solution phase using electron diffraction, a diffraction technique far better suited to detecting weak features of reciprocal space as a result of the much stronger interaction of electrons with matter.

We report here on complex modulated structures found to exist in a limited area of the solid solubility range, described by compositions around $Ni_{1.1}Sn_{0.7}P_{0.3}$.

2. EXPERIMENTAL

Preparation. Samples were prepared from weighed amounts of the elements (Ni, turnings from rods, 99.99%, Johnson, Matthey Laboratories Ltd.; Sn, granules, 99.9%, Fluka AG; P, lumps, 99.999%, Koch-Light Laboratories, Ltd.) by heating in evacuated silica glass ampoules. After a first heat treatment of 1 week at 1075 K, the samples were crushed, reannealed several times, and quenched in ice water from different temperatures, typically from 1125 K and 975 K.

Characterization. All samples were characterized by powder X-ray diffraction (PXD) using Guinier-Hägg cameras, Cu$K\alpha_1$ radiation, and Si as internal standard. Specimens for electron diffraction (ED) were prepared by crushing and dispersing onto holey, carbon-coated copper grids. The grids were examined in a JEOL 100CX transmission electron microscope.

3. RESULTS

Specimens Quenched from 1125 K

Specimens quenched from 1125 K of the $Ni_{1+m}Sn_{1-x}P_x$, B8-type phase field around the composition $Ni_{1.1}Sn_{0.7}P_{0.3}$ revealed an exceptionally complicated reciprocal lattice. Figure 2, for example, shows typical (a) [001], (b) $\langle 110\rangle$, (c) $\langle \bar{1}10\rangle$, (d) $\langle 111\rangle$, (e) $\langle \bar{1}11\rangle$, and (f) $\langle 112\rangle$ zone axis electron diffraction patterns (EDPs) of these specimens. No evidence was ever found for any breaking of hexagonal symmetry in such EDPs. Indexation is with respect to the strong Bragg reflections of the underlying $P6_3/mmc$, B8-type average structure (labeled **G** hereafter). In addition to these strong Bragg reflections, there exist a plethora of apparently sharp satellite reflections (see, for example, Figs. 2a, 2b, 2d, and 2f) and regions of more continuous diffuse streaking (see, for

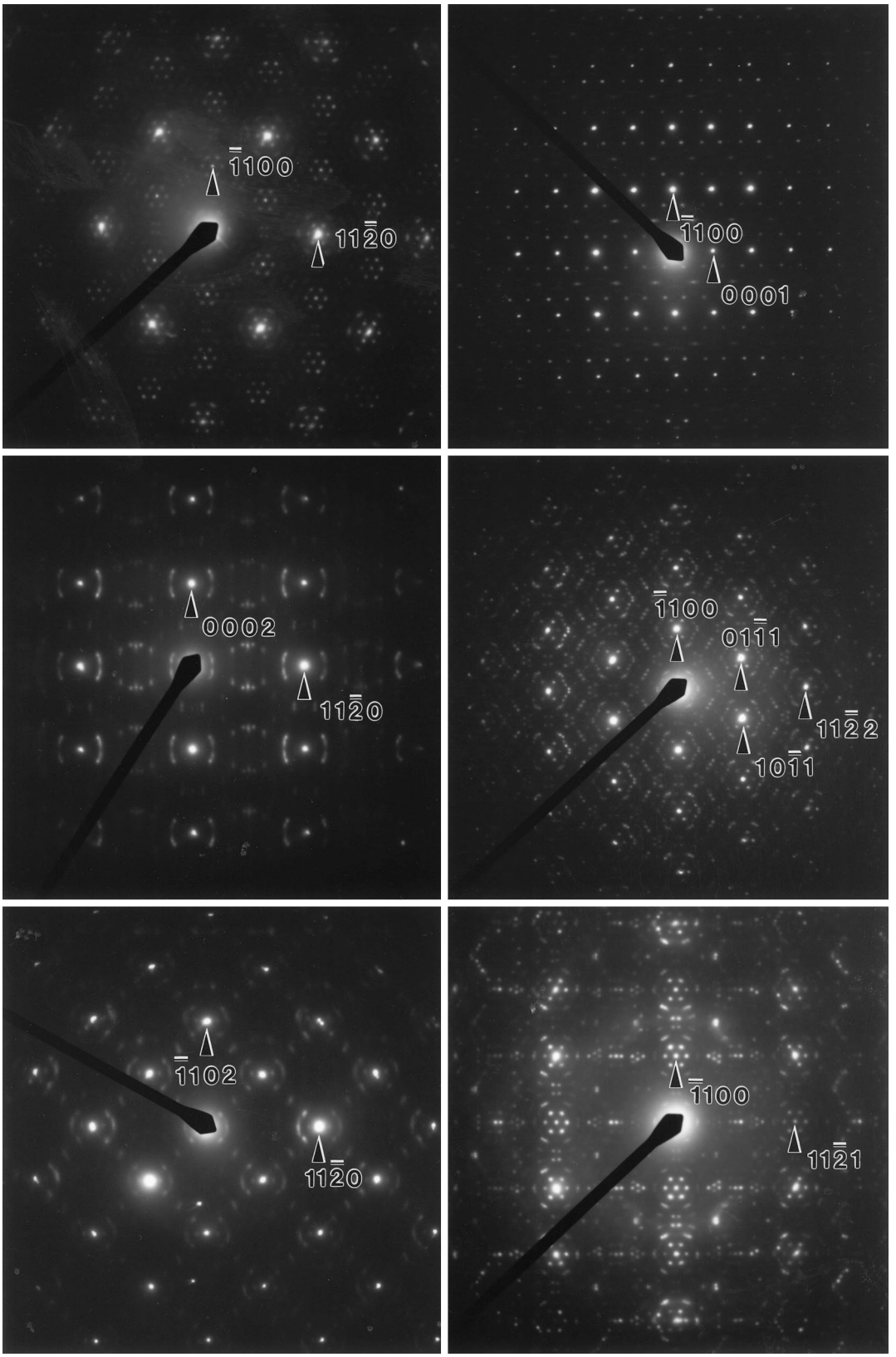

FIG. 2. Typical (a) [001], (b) ⟨110⟩, (c) ⟨$\bar{1}$10⟩, (d) ⟨111⟩, (e) ⟨$\bar{1}$11⟩, and (f) ⟨112⟩ zone axis EDPs characteristic of the $Ni_{1+m}Sn_{1-x}P_x$, B8-type phase field around the composition $Ni_{1.1}Sn_{0.7}P_{0.3}$ for specimens quenched from 1125 K. Indexation is with respect to the strong Bragg reflections of the underlying $P6_3/mmc$, B8-type average structure.

example, the arcs of diffuse intensity visible in Figs. 2c, 2e, and 2f). Clearly Sn/P and interstitial Ni ordering, and associated structural relaxation (although not totally long range ordered) does occur. Although it is not possible to fully index—let alone interpret—such complicated EDPs, there are some important features that should be pointed out.

In the [001] zone axis EDP of Fig. 2a, for example, there exists a prominent cluster of six apparently sharp satellite reflections surrounding each (generally strong) B8-type subcell reflection at $\mathbf{G} \pm \sim 0.09\langle 11\bar{2}0\rangle^*$. Somewhat more diffuse satellite reflections at $\mathbf{G} \pm \sim 2 \times 0.09\langle 11\bar{2}0\rangle^*$ are also present, as is a less prominent rectangular cluster of four apparent superlattice reflections centered on the $\mathbf{G} \pm \frac{1}{2}\langle \bar{1}100\rangle^*$ regions of reciprocal space at $\mathbf{G} \pm \frac{1}{2}\langle \bar{1}100\rangle^* \pm \sim 0.045\langle 1\bar{2}10\rangle^*$ and $\mathbf{G} \pm \frac{1}{2}\langle \bar{1}100\rangle^* \pm \sim 0.045\langle \bar{2}110\rangle^*$ respectively. Note that the $\mathbf{G} \pm \sim 0.09\langle 1\bar{2}10\rangle^*$ satellite reflections can thus be indexed as second harmonic satellite reflections of these latter satellite reflections. The appearance of what seems to be the same rectangular cluster of four satellite reflections along the $\mathbf{G} \pm \langle \bar{1}100\rangle^*$ directions of reciprocal space in Fig. 2d and particularly in Fig. 2f suggests that these satellite reflections are not confined to the $l = 0$ plane of reciprocal space but are part of a rather more extended (along c^*) arc of diffuse scattering.

The orthogonal $\{hh\bar{2}hl\}^*$ section of reciprocal space (see Fig. 2c) shows that the apparently sharp $\mathbf{G} \pm \sim 0.09\langle 11\bar{2}0\rangle^*$ and $\mathbf{G} \pm \sim 2 \times 0.09\langle 11\bar{2}0\rangle^*$ satellite reflections of Fig. 2a are likewise part of rather more extended (along c^*) arcs of diffuse scattering. Note, however, that the intensity in these arcs of diffuse scattering is not smoothly varying and appears to peak at positions on the arcs with noninteger c^* components. Note furthermore the characteristic extinction condition reflected in the fact that that the $\mathbf{G} \pm \sim 0.09\langle 11\bar{2}0\rangle^*$ "satellite" reflections (arcs of diffuse scattering) occur around the c glide forbidden $\langle hh\bar{2}hl\rangle^*$, l-odd positions of reciprocal space, whereas the $\mathbf{G} \pm \sim 2 \times 0.09\langle 11\bar{2}0\rangle^*$ "satellite" reflections (arcs of diffuse intensity) occur around the $\langle hh\bar{2}hl\rangle^*$, l-even positions of reciprocal space. Extinction conditions of this type are characteristic of many known binary B8-type superstructure phases (7, 8, 10).

It is important to note at this point that the reciprocal lattices of almost all known binary B8 type superstructure phases can be indexed as $\mathbf{H} = \mathbf{G} + m\mathbf{q}$, where the so-called primary modulation wave-vector $\mathbf{q}$ (11) is of the form $\langle hh\bar{2}hl\rangle^*$ (4, 7–10, 12). Indeed, even when B8-type structures are "disordered" (10), it is the case that the diffuse intensity distribution characteristic of the "disorder" is primarily located in $\{hh\bar{2}hl\}^*$ sections of reciprocal space. It is therefore perhaps not surprising that considerable scattering (in addition to the strong Bragg reflections of the underlying B8-type average structure) is observed in this $\{hh\bar{2}hl\}^*$ section of reciprocal space (see Fig. 2c).

Satellite reflections characterized by modulation wave-vectors of the form $\langle hh\bar{2}hl\rangle^*$ are not, however, the only type of satellite reflections observable in the EDPs of Fig. 2. In the $\langle 110\rangle$ zone axis EDP of Fig. 2b, for example, sharp satellite reflections at $\mathbf{G} \pm \frac{1}{4}\langle \bar{1}101\rangle^*$ are observable along with more diffuse second harmonic satellite reflections centered on $\mathbf{G} \pm \frac{1}{2}\langle \bar{1}101\rangle^*$. These $\mathbf{G} \pm \frac{1}{4}\langle \bar{1}101\rangle^*$ type of satellite reflections are also visible in the $\langle \bar{1}11\rangle$ zone axis EDP of Fig. 2e, where it is apparent that they are again part of a more continuous arc of diffuse intensity.

The highest density of satellite reflections in Fig. 2, however, occurs along $\mathbf{G} \pm \langle 11\bar{2}1\rangle^*$ directions of reciprocal space whenever $\langle 11\bar{2}1\rangle^*$ reflections of the B8 average structure are excited in the Zero Order Laue Zone (or ZOLZ) as, for example, in the $\langle \bar{1}10\rangle$ zone axis EDP of Fig. 2c (where one such $\langle 11\bar{2}1\rangle^*$ type of reflection is excited), the $\langle 111\rangle$ zone axis EDP of Fig. 2d (where two such $\langle 11\bar{2}1\rangle^*$ reflections are simultaneously excited), and the $\langle 112\rangle$ zone axis EDP of Fig. 2f (where one such $\langle 11\bar{2}1\rangle^*$ type of reflection is excited). Along such $\mathbf{G} \pm \langle 11\bar{2}1\rangle^*$ directions of reciprocal space, there are invariably satellite reflections observed at $\mathbf{G} \pm \frac{m}{11}\langle 11\bar{2}1\rangle^*$, where m is an integer. This is particularly apparent in Fig. 2f, but also in Fig. 2d and, to a rather lesser extent, in Fig. 2c. (Note, however, that an additional satellite reflection at $\mathbf{G} \pm \frac{1}{2}\langle 11\bar{2}1\rangle^*$ is also observed). Such $\frac{m}{11}\langle 11\bar{2}1\rangle^*$ modulations occur along all six symmetry equivalent $\langle 11\bar{2}1\rangle^*$ reciprocal lattice directions in specimens quenched from higher temperatures. Thus in Fig. 2d, for example, $\frac{m}{11}\langle 11\bar{2}1\rangle^*$ modulations occur along both symmetry-equivalent $\langle 11\bar{2}1\rangle^*$ reciprocal lattice directions excited in the ZOLZ for this particular zone axis orientation.

Specimens Quenched from 975 K

When specimens quenched from 975 K around the composition $Ni_{1.1}Sn_{0.7}P_{0.3}$ were examined, it was apparent that a complicated, long range ordered, superstructure phase had condensed out that was nonetheless closely related to the phase existing at higher temperature. Figure 3, for example, shows (a) $[\bar{1}10]$, (b) [101], (c) [110], and (d) [112] zone axis EDPs (indexed in an internally self-consistent manner with respect to the underlying B8-type average structure) of these specimens for direct comparison with Figs. 2c, 2d, 2b, and 2f respectively. (Square rather than angled brackets are used because there are no longer symmetry equivalent zone axis orientations).

Detailed tilting experiments show that the symmetry of reciprocal space has been reduced from hexagonal to triclinic. Remarkably the cell dimensions of the underlying B8-type average structure remain metrically hexagonal so that at least 12, and possibly 24, distinct twins whose B8 average substructure reflections overlap exactly are to be expected. Microdiffraction patterns rather than selected area EDPs were therefore taken to minimize the possibility of twinning. Twinning was indeed often apparent in the TEM. Somewhat surprisingly, however, it did not prove

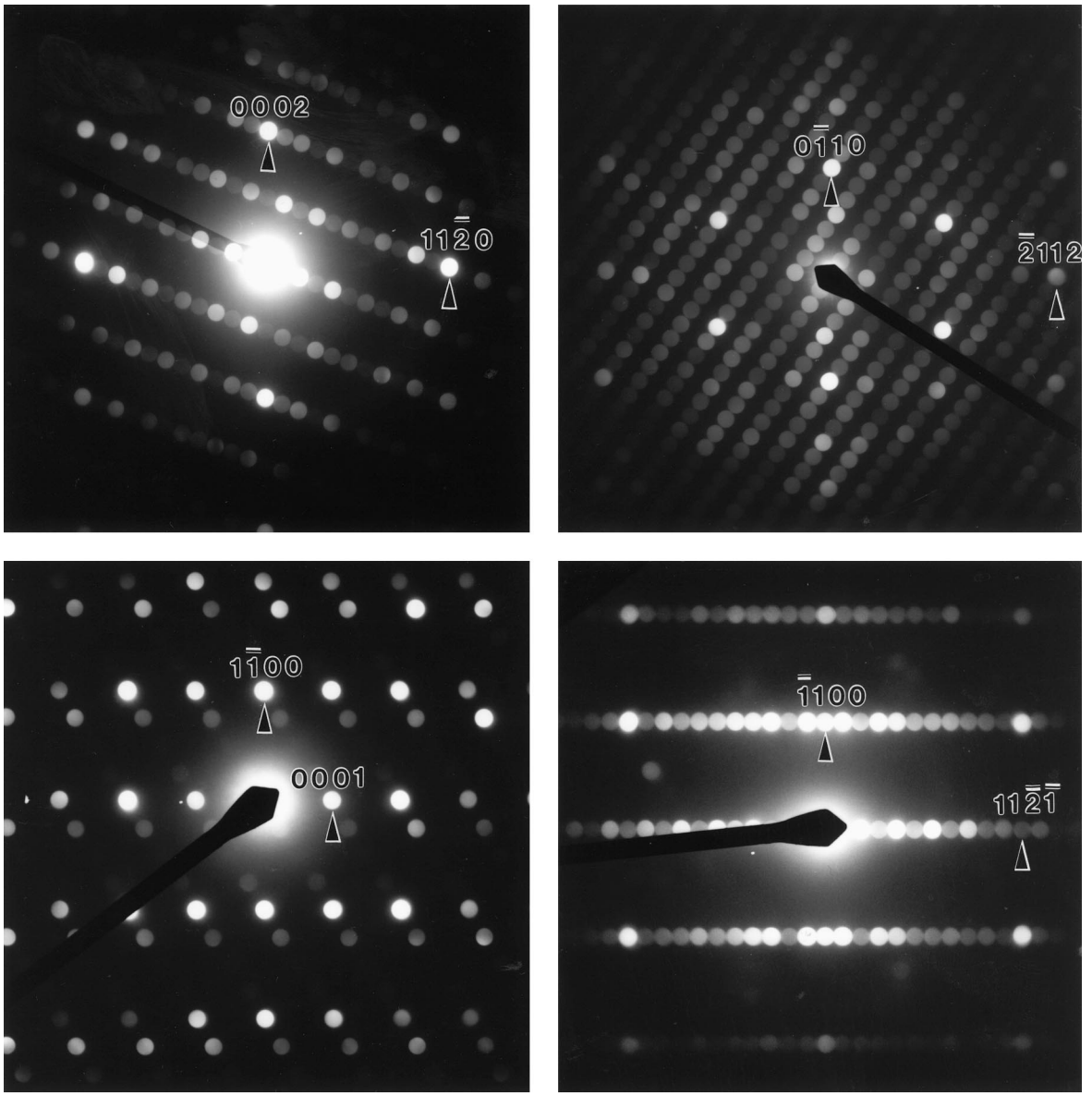

FIG. 3. (a) [$\bar{1}$10], (b) [101], (c) [110], and (d) [112] zone axis EDPs (indexed in an internally self-consistent manner with respect to the underlying B8-type average structure) of the $Ni_{1+m}Sn_{1-x}P_x$, B8 type phase field around the composition $Ni_{1.1}Sn_{0.7}P_{0.3}$ for specimens quenched from 975 K.

too difficult to obtain single crystal EDPs, provided appropriate care was taken and the microdiffraction technique used.

The results of careful investigation showed that all observed reflections could be fully indexed as $\mathbf{H} = \mathbf{G} + m\mathbf{q}_1 + n\mathbf{q}_2$, where m and n are integers and where $\mathbf{q}_1 = \frac{1}{11}[11\bar{2}\bar{1}]^*$ and $\mathbf{q}_2 = \frac{1}{22}[5\bar{6}1\bar{5}]^*$ respectively. The only zone axis at which $\mathbf{q}_1$ and $\mathbf{q}_2$ are simultaneously excited in the ZOLZ is the [101] zone axis EDP of Fig. 3b. Note that $\mathbf{q}_2$ is very nearly, but not quite, equal to $-\frac{1}{4}\langle\bar{1}101\rangle^*$, which explains the similarities but also the differences between Fig. 2b and Fig. 3c, *i.e.*, the $\mathbf{G} \pm \mathbf{q}_2$ satellite reflections are almost but not quite in the ZOLZ at the [110] zone axis orientation of Fig. 3c and hence occur preferentially to one side of the B8 subcell Bragg reflections $\mathbf{G}$ away from the exact center of the pattern as a result of the slight upward curvature of the Ewald sphere. This slight deviation of $\mathbf{q}_2$ from $-\frac{1}{4}\langle\bar{1}101\rangle^*$ may also expain why the $\mathbf{G} \pm \frac{1}{2}[11\bar{2}\bar{1}]^*$ satellite reflections apparent in Fig. 2f are missing in Fig. 3d, *i.e.*, $[01\bar{1}0]^* + 2\mathbf{q}_2$ now equals $\frac{5}{11}[11\bar{2}\bar{1}]^*$ rather than the $\frac{1}{2}[11\bar{2}\bar{1}]^*$ it would equal were $\mathbf{q}_2$ equal to $-\frac{1}{4}\langle\bar{1}101\rangle^*$ exactly.

The use of $\mathbf{q}_1$ in the above indexation scheme emphasizes the relationship of the reciprocal lattice of $Ni_{1.1}Sn_{0.7}P_{0.3}$ to those of $T_{1+m}B$ binary phases where primary modulation

wave-vectors are almost invariably of the form $\langle hh2\bar{h}l\rangle^*$ (4, 7–9, 12). This $\mathbf{H} = \mathbf{G} + m\mathbf{q}_1 + n\mathbf{q}_2$ indexation scheme is not, however, strictly necessary and only one so-called "primary" modulation wave-vector is really required. Given that $\mathbf{G} - 4\mathbf{q}_2 = \mathbf{G} + [\bar{1}101]^* + \mathbf{q}_1$ (see Fig. 3b), for example, it is clear that observed reflections can be equally well indexed by $\mathbf{H} = \mathbf{G} + m\mathbf{q}$, where m is an integer and $\mathbf{q} = \frac{1}{22}\,[5\bar{6}1\bar{5}]^*$, (or indeed by $\mathbf{H} = \mathbf{G} + m\mathbf{q}$, where $\mathbf{q} = \frac{1}{22}\,[5\bar{6}1\bar{5}]^* + \frac{n}{11}\,[11\bar{2}1]^*$ and $n = -2, -1, 0, +1,$ or $+2$) (see Fig. 3b).

Ordinarily one would choose n, and hence the so-called "primary" modulation wave-vector $\mathbf{q}$, such that the intensity of observed satellite reflections $\mathbf{G} + m\mathbf{q}$ drops off systematically with increasing harmonic order m. The corresponding compositional and displacing AMFs would then be much more likely to have a directly interpretable form (11). In the current case, almost all harmonic orders are observed relatively strongly (consistent with the notion of square, wave-like compositional AMFs (11)), so it is difficult to recognize what an appropriate choice for n should be. The fact that the strongest satellite reflections in Fig. 3b occur in a band close to the $[0\bar{1}10]^*$ direction of reciprocal space and the strongest of these satellite reflections, for a sufficiently thin crystal, is invariably the $[0\bar{1}10]^* - (\frac{1}{22}\,[5\bar{6}1\bar{5}]^* - \frac{2}{11}\,[11\bar{2}1]^*)$ reflection suggests that the appropriate choice is $n = -2$, corresponding to $\mathbf{q} = \frac{1}{22}\,[1,\ \bar{1}0,\ 9,\ \bar{1}]^* = \frac{1}{2}\,[0\bar{1}10]^* + \frac{1}{22}\,[11\bar{2}1]^*$. Note that just such satellite reflections (along with their 6/*mmm* symmetry-equivalent variants) are also present in Fig. 2d and that $\mathbf{G} \pm \frac{m}{11}\,\langle 11\bar{2}1\rangle^*$ satellite reflections therefore correspond to even order (*i.e.*, $m = 2, 4, ..$) satellite reflections.

The rows of 11 satellite reflections along the $\mathbf{G} \pm \langle 11\bar{2}1\rangle^*$ directions of reciprocal space at $\mathbf{G} \pm \frac{m}{11}\langle 11\bar{2}1\rangle^*$ in Figs. 2d, 2f and, to a lesser extent, 2c are still present in Figs. 3b, 3d, and 3a, respectively, but now only along the $[11\bar{2}1]^*$ direction. The differences in appearance of Figs. 2d, 2f, and 2c from Figs. 3b, 3d, and 3a are thus due to the fact that the $\frac{m}{11}\,\langle 11\bar{2}1\rangle^*$ modulations now occur along only one of the six originally symmetry-equivalent $\langle 11\bar{2}1\rangle^*$ directions of reciprocal space. (It thus appears that all of the reflections observed in the specimens quenched from higher temperatures can be accounted for in terms of microdomain twinning of the low temperature superstructure phase). Note the pseudoextinction condition apparent in Fig. 3a, *i.e.*, the $\mathbf{G} \pm \frac{(2m+1)}{11}\,\langle 11\bar{2}1\rangle^*$ satellite reflections are clearly strongest around the B8, c glide forbidden $\mathbf{G} = \langle hh2\bar{h}l\rangle^*$, l odd positions of reciprocal space, whereas the $\mathbf{G} \pm \frac{2m}{11}\,\langle 11\bar{2}1\rangle^*$ satellite reflections are clearly strongest around the $\langle hh2\bar{h}l\rangle^*$, l even positions. This mirrors the characteristic extinction condition of Fig. 2c, in which the $\mathbf{G} \pm \sim 0.09\langle 11\bar{2}0\rangle^*$ "satellite" reflections occur around the c glide forbidden $\langle hh2\bar{h}l\rangle^*$, l odd positions of reciprocal space, whereas the $\mathbf{G} \pm \sim 2 \times 0.09\langle 11\bar{2}0\rangle^*$ "satellite" reflections/arcs of diffuse intensity occur around the $\langle hh2\bar{h}l\rangle^*$, l even positions of reciprocal space.

As mentioned above, the reciprocal lattices of almost all known binary B8-type superstructure phases can be indexed as $\mathbf{H} = \mathbf{G} + m\mathbf{q}$, where the (usually, but not always, single) so-called primary modulation wave-vector $\mathbf{q}$ is invariably of the form $\langle hh2\bar{h}l\rangle^*$ (4, 7–9, 12). In the cases of η^6- and η^8-Cu_5Sn_4 (8), for example, the primary modulation wave-vectors are of the form $\mathbf{q} = \frac{1}{3}\,(\mathbf{a}^* + \mathbf{b}^*) + \frac{1}{2}\,\mathbf{c}^*$ and $\mathbf{q} = \frac{3}{8}\,(\mathbf{a}^* + \mathbf{b}^*) + \frac{1}{2}\,\mathbf{c}^*$ respectively (*cf.* Figs. 3a and 3c and Figs. 5a and 5c of (8) with Fig. 3a).

Perhaps the closest similarity that the reciprocal lattice of low temperature $Ni_{1.1}Sn_{0.7}P_{0.3}$ has to the reciprocal lattice of a known binary superstructure phase is with the η'-Cu_6Sn_5 superstructure phase (cf. Fig. 2c and 2f of (7) with Figs. 3b and 3d of (7)). The resultant (subscript R) $C2/c$, $\mathbf{a}_R = \mathbf{a} + \mathbf{b} + 2\mathbf{c}$, $\mathbf{b}_R = -\mathbf{a} + \mathbf{b}$, $\mathbf{c}_R = 2\mathbf{a} + 2\mathbf{b} + \mathbf{c}$ supercell of η'-Cu_6Sn_5 (7) corresponds to reciprocal space basis vectors $\mathbf{a}_R^* + \mathbf{b}_R^* = \mathbf{b}^* - \frac{2}{5}\,[11\bar{2}1]^*$, $\mathbf{a}_R^* - \mathbf{b}_R^* = \mathbf{a}^* - \frac{2}{5}\,[11\bar{2}1]^*$, and $\mathbf{c}_R^* = \frac{1}{5}\,[11\bar{2}1]^*$, so that reciprocal space can be fully indexed as $\mathbf{H} = \mathbf{G} + m\mathbf{q}$, with primary modulation wave-vector $\mathbf{q} = \frac{1}{5}\,[11\bar{2}1]^*$.

$C2/c$ resultant space group symmetry for η'-Cu_6Sn_5 requires that $F(h0l) = 0$ unless h and l are both even so that, at $[010]_R = [\bar{1}10]$ zone axis orientations, $\mathbf{G} \pm \frac{(2m+1)}{5}\,[11\bar{2}1]^*$ satellite reflections only occur around the B8, c glide forbidden $\mathbf{G} = [hh2\bar{h}l]^*$, l odd positions of reciprocal space, whereas the $\mathbf{G} \pm \frac{2m}{5}\,[11\bar{2}1]^*$ satellite reflections only occur around the $[hh2\bar{h}l]^*$, l even positions. As already mentioned above, a similar pseudoextinction condition is characteristic of $Ni_{1.1}Sn_{0.7}P_{0.3}$ (see Fig. 3a). While this is clearly an important similarity implying a specific phase relationship between the compositional and displacive AMFs (11) of c glide related atom sites, at least in projection along $[\bar{1}10]$ (see below), there is also a sharp distinction in that the reciprocal lattice of low temperature $Ni_{1.1}Sn_{0.7}P_{0.3}$ cannot be fully indexed as $\mathbf{H} = \mathbf{G} + m\mathbf{q}$, with $\mathbf{q} = \frac{1}{11}\,[11\bar{2}1]^*$. The appropriate primary modulation wave-vector is rather $\mathbf{q} = \frac{1}{22}\,[1, \bar{1}0, 9, \bar{1}]^* = \frac{1}{2}\,[0\bar{1}10]^* + \frac{1}{22}\,[11\bar{2}1]^*$. Such a primary modulation wave-vector has not been reported to date for any known binary compound.

In conventional crystallographic terms, the resultant triclinic reciprocal space unit cell vectors can be chosen to be $\mathbf{a}_R^* = \mathbf{q}_2 + n\mathbf{q}_1 = \frac{1}{22}\,([5 + 2n]\mathbf{a}^* + [-6 + 2n]\mathbf{b}^* + [-5 - 2n]\mathbf{c}^*)$, $\mathbf{b}_R^* = \mathbf{q}_1$, $\mathbf{c}_R^* = \mathbf{c}^*$ (subscript R for resultant triclinic cell). The corresponding real space triclinic resultant unit cell vectors in terms of those of the underlying B8 average structure are then given by $\mathbf{a}_R = 2\mathbf{a} - 2\mathbf{b}$, $\mathbf{b}_R = (6 - 2n)\mathbf{a} + (5 + 2n)\mathbf{b}$ and $\mathbf{c}_R = \mathbf{a} + \mathbf{c}$ respectively. In terms of keeping γ as close as possible to 90°, one should perhaps choose $n = 0$. Given underlying B8 average structure unit cell dimensions for this specimen of $a = 3.806$, $c = 5.215$Å, the resultant triclinic unit cell dimensions for this choice of setting become $a_R = 13.184$, $b_R = 21.191$, $c_R = 6.456$Å, $\alpha_R = 68.248°$, $\beta_R = 59.300°$, and $\gamma_R = 81.052°$. Such a triclinic supercell contains 22 average B8 type unit cells.

4. A STRUCTURAL MODEL FOR $Ni_{1.1}Sn_{0.7}P_{0.3}$

The average B8 cell dimensions imply that Ni atoms in trigonal bipyramidal holes are surrounded by three nonmetal neighbors at average distances of $a/\sqrt{3} \sim 2.20$ Å and two at $c/2 \sim 2.60$ Å. Given that normal Ni-P distances are $\sim$2.2 Å, whereas normal Ni–Sn distances are $\sim$2.6Å, Furuseth and Fjellvåg (6) suggested that a preferred clustering is highly likely to take place around the filled interstitial Ni sites, giving rise to NiP_3Sn_2 units with the P atoms in the triangular base of the trigonal bipyramids and the Sn atoms in the apical positions. Such an arrangement would minimize the inevitable strain accompanying the insertion of an interstitial Ni atom and thus would seem crystal chemical common sense. It was presumed in (6) that these NiP_3Sn_2 units did not agglomerate into larger clusters because of the lack of diffraction evidence for any superstructure ordering. Given the electron diffraction evidence and the above crystal chemical considerations, it seems most likely that the observed low temperature superstructure phase must arise principally as a result of ordering of such NiP_3Sn_2 units.

The triclinic unit cell given above implies that these NiP_3Sn_2 structural units are able to come as close as $\mathbf{c}_R = \mathbf{a} + \mathbf{c}$ to each other (presumably the strain interaction between neighboring NiP_3Sn_2 units is minimal for this particular separation distance) but, on the other hand, studiously avoid an $(\mathbf{a} - \mathbf{b})$ separation distance. The doubling of the B8 repeat distance along the $(\mathbf{a} - \mathbf{b})$ direction is a major distinction between the current $Ni_{1.1}Sn_{0.7}P_{0.3}$ ternary B8 phase, and known binary B8 phases and represents the real space analog of the fact that the primary modulation wave-vector cannot be expressed in the form $\langle hh\bar{2}hl\rangle^*$.

Given that the high temperature $Ni_{1+m}Sn_{1-x}P_x$, B8-type phase field was found by Furuseth and Fjellvåg (6) to separate out as an isolated B8-type phase region of rather narrow compositional range at low temperatures, it seems likely that the low temperature phase may in fact be a line phase of fixed composition rather close to $Ni_{1.1}Sn_{0.7}P_{0.3}$. The fact that four isolated NiP_3Sn_2 units per resultant triclinic supercell would predict a resultant composition of $Ni_{48}Sn_{32}P_{12}$ or $Ni_{1.091}Sn_{0.727}P_{0.273}$ (remember that the resultant triclinic supercell contains 22 average B8 type unit cells) very close to this confirms the reasonableness of the proposition that the superstructure is due to ordering of NiP_3Sn_2 units. The question becomes which four of the potential 44 interstitial Ni atom sites per resultant triclinic supercell are occupied. (Note that triangular base, corner-connected NiP_3Sn_2 units would give rise to a resultant stoichiometry of $Ni_{48}Sn_{34}P_{10}$ or $Ni_{1.091}Sn_{0.773}P_{0.227}$, which is close to, but perhaps a little too far removed from, the observed stoichiometry of $Ni_{1.1}Sn_{0.7}P_{0.3}$ (6)).

Two pieces of evidence are used here to propose a plausible model for the resultant triclinic supercell. The first is the pseudoextinction condition of Fig. 3a as discussed above. The presence of a similar, but this time exact, extinction condition in the case of η'-Cu_6Sn_5 (corresponding to the resultant c glide) suggests an important structural relationship between symmetry-related interstitial sites in both cases. In the case of η'-Cu_6Sn_5 (7), the fivefold superstructure along $[11\bar{2}1]^*$ was attributed to a filling of all Edshammar sites in every fifth $[11\bar{2}1]$ plane. (Note that filled interstitial Ni sites are surrounded by 5 nonmetal atoms and 6 metal atoms so the overall coordination polyhedron can be described as an 11-coordinate Edshammar polyhedron). Per average B8 unit cell, there are two c glide related Edshammar sites labeled E_a and E_b; E_a at $\mathbf{r}_a = \frac{2}{3}\mathbf{a} + \frac{1}{3}\mathbf{a} - \frac{1}{4}\mathbf{c}$ and E_b at $\mathbf{r}_b = \frac{1}{3}\mathbf{a} + \frac{2}{3}\mathbf{a} + \frac{1}{4}\mathbf{c}$ (see Fig. 1). Similarly there exist two sets of $(11\bar{2}1)$ planes (labeled E_a and E_b planes because they run through only E_a or E_b sites respectively) per average B8 unit cell. The resultant c glide extinction condition of η'-Cu_6Sn_5 (7) arises because of a very specific phase relationship between these E_a and E_b $(11\bar{2}1)$ planes such that the filled E_b $(11\bar{2}1)$ planes occur exactly midway between the filled E_a $(11\bar{2}1)$ planes and vice versa (see Fig. 3 of (7)). The pseudoextinction condition of Fig. 3a shows that the structure of $Ni_{1.1}Sn_{0.7}P_{0.3}$ in projection along $[\bar{1}10]$ must be rather close to obeying a similar constraint, *i.e.*, the filled E_b $(11\bar{2}1)$ planes must occur close to midway (although not exactly midway) between the filled E_a $(11\bar{2}1)$ planes and vice versa.

The second piece of evidence used to propose a plausible model for the resultant triclinic supercell is the observation that the strongest satellite reflection in [101] zone axis EDPs, such as Fig. 3b, is invariably the $[0\bar{1}10]^* - (\frac{1}{22}[5\bar{6}1\bar{5}]^* - \frac{2}{11}[11\bar{2}1]^*) = \frac{1}{22}[\bar{1}, \bar{1}2, 13, 1]^*$ reflection (in the kinematical limit of a sufficiently thin crystal), suggesting that the filled E_a and E_b sites must lie rather close to $(\bar{1}, \bar{1}2, 13, 1)$ lattice planes.

Putting these two pieces of evidence together, along with the assumption that the NiP_3Sn_2 units are not corner-connected, the most plausible model for the distribution of occupied interstitial sites is that shown in Figs. 4a and 4b. The resultant space group symmetry is $P\bar{1}$ with occupied interstitial E_a sites at $\mathbf{r}_a + 3\mathbf{a} + 3\mathbf{b}$ and $\mathbf{r}_a + 5\mathbf{a} + 3\mathbf{b}$ and occupied interstitial E_b sites at $\mathbf{r}_b + \mathbf{b}$ and $\mathbf{r}_b + 2\mathbf{a} + \mathbf{b}$, respectively. Note that the inversion center in the proposed resultant structure is located at $-\frac{1}{2}\mathbf{a}$ with respect to the origin used in Figs. 1 and 4, where it is indicated by the cross. For the purposes of clarity, only the interstitial Ni sites (the filled circles) are marked in Fig. 4a. It is understood that the nonmetal atom sites in the triangular base of the surrounding trigonal bipyramids are filled with P atoms, while the apical nonmetal atom sites are filled with Sn atoms.

Because $\mathbf{c}_R = \mathbf{a} + \mathbf{c}$, only one resultant triclinic supercell (corresponding to one octahedral layer of the B8 subcell) is shown in projection along $\mathbf{c}$ in Fig. 4a. The basal plane unit cells of both the triclinic superstructure $(\mathbf{a}_R = 2\mathbf{a} - 2\mathbf{b},$

$\mathbf{b}_R = 6\mathbf{a} + 5\mathbf{b}$) and the B8 substructure are outlined. The distribution of occupied interstitial sites in the neighboring octahedral layer (in projection along **c**) would be exactly the same as that shown in Fig. 4a, but translated by **a** (the supercell unit cell repeat vector $\mathbf{c}_R = \mathbf{a} + \mathbf{c}$). The trace of a ($\bar{1}$, $\bar{1}\bar{2}$, 13, 1) lattice plane running through the occupied interstitial Ni sites is shown in Fig. 4a and it can be seen that the filled E_a and E_b sites do indeed lie rather close to ($\bar{1}$, $\bar{1}\bar{2}$, 13, 1) lattice planes as suggested by the experimental observation that the strongest satellite reflection in Fig. 3b is always the $\frac{1}{22}$ [$\bar{1}$, $\bar{1}\bar{2}$, 13, 1]* reflection. Note that ($\mathbf{a} - \mathbf{b}$) is not a resultant unit cell vector as filled and empty sites alternate on translation by ($\mathbf{a} - \mathbf{b}$) in Fig. 4a.

The same model is shown in projection along [$\bar{1}$10] in Fig. 4b. There are two (out of 11 possible) half-filled E_a and two (again out of 11 possible) half-filled E_b ($11\bar{2}\bar{1}$) lattice planes per supercell repeat distance along [$11\bar{2}\bar{1}$]*. (Note that ($11\bar{2}\bar{1}$) lattice planes are either half-filled or completely empty, *i.e.*, filled and empty sites alternate on translation by ($\mathbf{a} - \mathbf{b}$) in the half-filled ($11\bar{2}\bar{1}$) lattice planes of Fig. 4a). The half-filled E_a and E_b ($11\bar{2}\bar{1}$) lattice planes occur close to midway (but not exactly midway) between the filled E_a ($11\bar{2}\bar{1}$) planes and vice versa, so the proposed model is also compatible with the pseudoextinction condition of Fig. 3a. (Note that it is quite possible to generate a closely related model in which the extinction condition would be obeyed exactly by translating the filled E_b sites of Fig. 4a by $+\mathbf{a}$ relative to the filled E_a sites. Such a translation has the effect of translating the half-filled E_b ($11\bar{2}\bar{1}$) lattice planes to exactly midway between the half-filled E_a ($11\bar{2}\bar{1}$) lattice planes

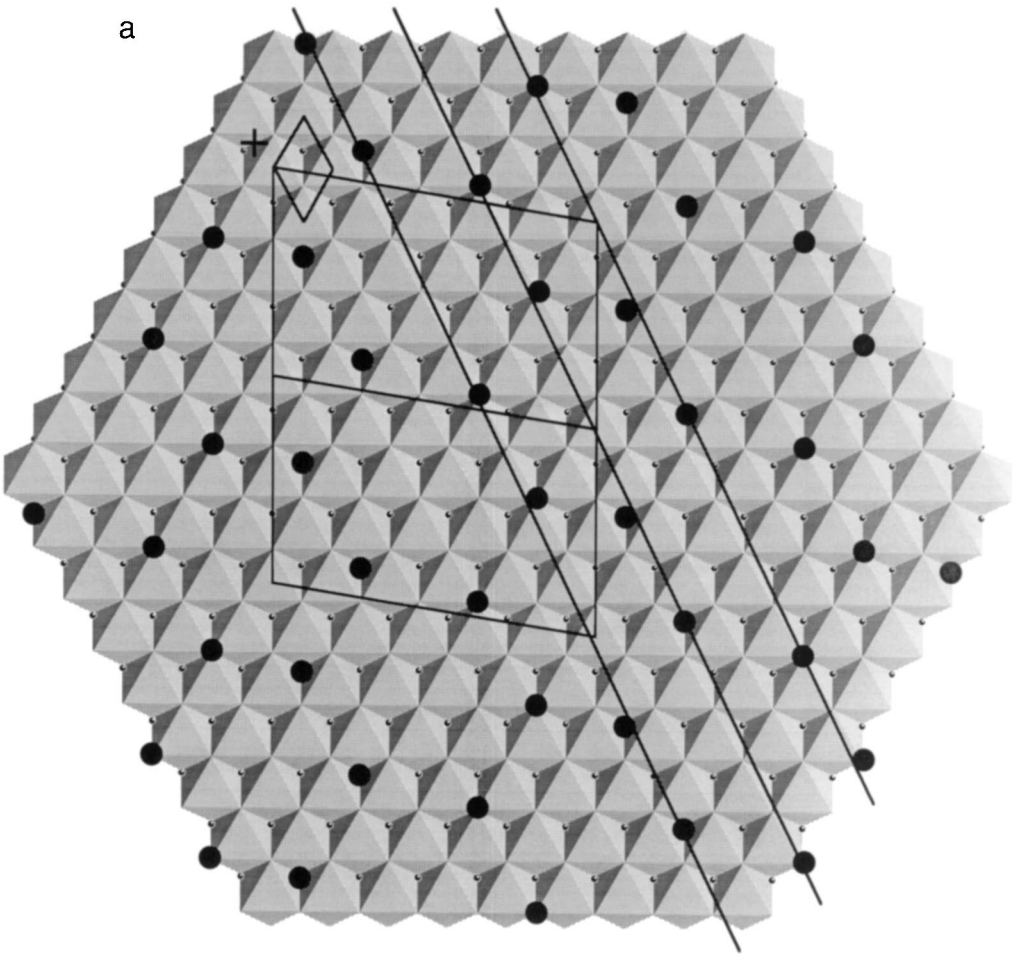

FIG. 4. Plausible model for the distribution of occupied interstitial Ni atom sites in the resultant supercell. Space group symmetry is $P\bar{1}$ with occupied interstitial E_a sites at $\mathbf{r}_a + 3\mathbf{a} + 3\mathbf{b}$ and $\mathbf{r}_a + 5\mathbf{a} + 3\mathbf{b}$ and occupied interstitial E_b sites at $\mathbf{r}_b + \mathbf{a} - \mathbf{b}$ and $\mathbf{r}_b + 3\mathbf{a} - \mathbf{b}$ respectively. The trace of some occupied ($\bar{1}$, $\bar{1}\bar{2}$, 13, 1) lattice planes is shown. Because $\mathbf{c}_R = \mathbf{a} + \mathbf{c}$, only one resultant triclinic supercell (corresponding to one octahedral layer of the B8 subcell) is shown in projection along **c** in (a). The basal plane triclinic unit cell and that of the B8 substructure are outlined. The same model is shown in projection along [$\bar{1}$10] in (b). The two (out of 11 possible) half-filled E_a and two (again out of 11 possible) half-filled E_b ($11\bar{2}\bar{1}$) lattice planes per supercell repeat distance along [$11\bar{2}\bar{1}$]* are shown. Note that the half-filled E_a and E_b ($11\bar{2}\bar{1}$) lattice planes occur close to midway (but not exactly midway) between the filled E_a ($11\bar{2}\bar{1}$) planes and vice versa. The projected triclinic unit cell is outlined.

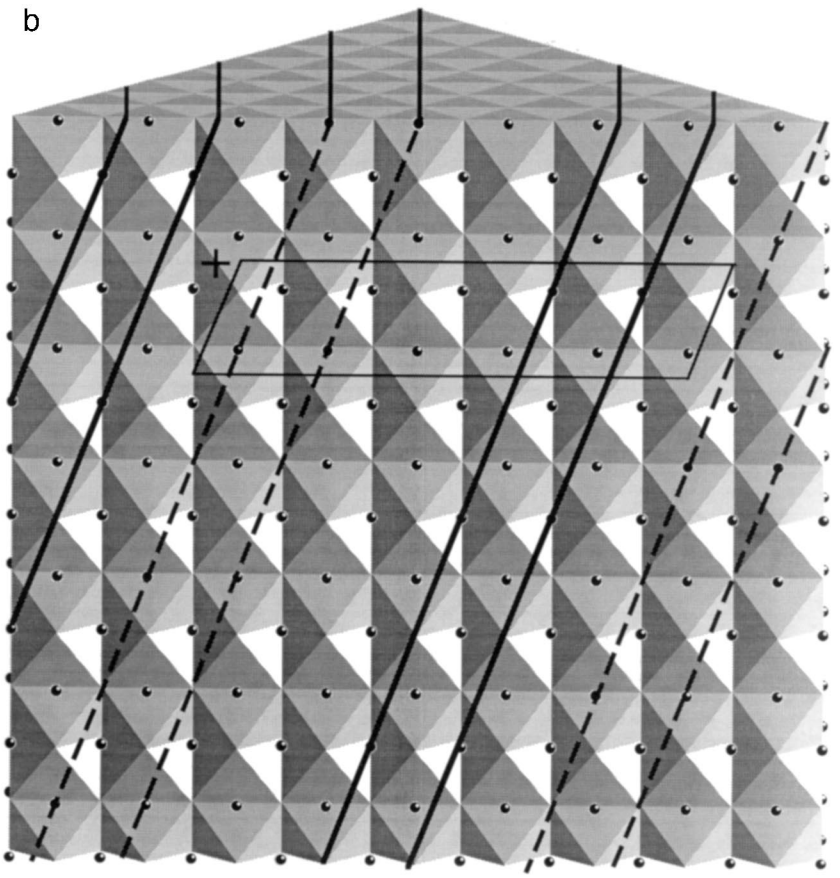

FIG. 4—*Continued*

and vice versa. The proposed model represents the closest that the E_b ($11\bar{2}\bar{1}$) planes can come to being exactly midway between the half-filled E_a ($11\bar{2}\bar{1}$) lattice planes without the extinction condition being exact).

While the proposed model is undoubtedly plausible and apparently compatible with the observed electron diffraction evidence, the authors acknowledge that it may not necessarily be the only possible such model. Further progress must await the results of a full "single crystal" X-ray structure refinement. Given the hexagonal subcell symmetry and the consequent near inevitability of extensive twinning, such a refinement will be by no means a trivial exercise.

ACKNOWLEDGMENT

Dr. A-K. Larsson gratefully acknowledges financial support from STINT via the Swedish Natural Science Research Council (NFR).

REFERENCES

1. P. Villars and L. D. Calvert (Eds.), "Pearson's Handbook of Crystallographic Data for Intermetallic Phases." ASM, Cleveland, Ohio, 1992.
2. M. Hansen (Ed.), "Constitution of the Binary Alloys." McGraw-Hill, New York, 1958.
3. A. Kjekshus and W. B. Pearson, *Prog. Solid State Chem.* **1,** 83 (1964).
4. S. Lidin and A-K. Larsson, *J. Solid State Chem.* **118,** 313 (1995).
5. S. Furuseth and H. Fjellvåg, *Acta Chem. Scand. A* **39,** 537 (1985).
6. S. Furuseth and H. Fjellvåg, *Acta Chem. Scand.* **48,** 134 (1994).
7. A-K. Larsson, L. Stenberg, and S. Lidin, *Acta Crystallogr. Sect. B* **50,** 636 (1994).
8. A-K. Larsson, L. Stenberg, and S. Lidin, *Z. Krist.* **210,** 832 (1995).
9. M. Elding-Pontén, L. Stenberg, A-K. Larsson, S. Lidin, and K. Ståhl, *J. Solid State Chem.* **129**, 231–241 (1997).
10. A-K. Larsson, R. L. Withers, and L. Stenberg, *J. Solid State Chem.* **127**, 222 (1996).
11. J. M. Pérez-Mato, G. Madariaga, F. J. Zúñiga, and A. Garcia Arribas, *Acta Crystallogr. Sect. A* **43**, 216–226, 1987.
12. A-K. Larsson and R. L. Withers, *J. Alloys and Compounds*, in press (1997).